

Limitations of quantitative photoacoustic measurements of blood oxygenation in small vessels

Mathangi Sivaramakrishnan¹, Konstantin Maslov¹, Hao F Zhang¹,
George Stoica² and Lihong V Wang¹

¹ Optical Imaging Laboratory, Department of Biomedical Engineering, Texas A&M University
3120 TAMU, College Station, TX 77843-3120, USA

² Department of Pathobiology, Texas A&M University, College Station, TX 77843-5547, USA

E-mail: LWang@bme.tamu.edu

Received 15 June 2006, in final form 3 January 2007

Published 8 February 2007

Online at stacks.iop.org/PMB/52/1349

Abstract

We investigate the feasibility of obtaining accurate quantitative information, such as local blood oxygenation level (sO_2), with a spatial resolution of about 50 μm from spectral photoacoustic (PA) measurements. The optical wavelength dependence of the peak values of the PA signals is utilized to obtain the local blood oxygenation level. In our *in vitro* experimental models, the PA signal amplitude is found to be linearly proportional to the blood optical absorption coefficient when using ultrasonic transducers with central frequencies high enough such that the ultrasonic wavelengths are shorter than the light penetration depth into the blood vessels. For an optical wavelength in the 578–596 nm region, with a transducer central frequency that is above 25 MHz, the sensitivity and accuracy of sO_2 inversion is shown to be better than 4%. The effect of the transducer focal position on the accuracy of quantifying blood oxygenation is found to be negligible. *In vivo* oxygenation measurements of rat skin microvasculature yield results consistent with those from *in vitro* studies, although factors specific to *in vivo* measurements, such as the spectral dependence of tissue optical attenuation, dramatically affect the accuracy of sO_2 quantification *in vivo*.

1. Introduction

Blood oxygenation level is an important physiological measure of cardio-vascular function on the macro level, but it can also provide information on localized tissue oxygenation at the microvasculature level. Oxygenation level is an important factor for the healing of burns (Venkatesh *et al* 2001) and wounds (Gottrup 2004), and it can also influence the effectiveness of chemo- and radio-therapies in cancer treatment (Henke *et al* 2000). Correspondingly,

localized non-invasive oxygenation measurements in the skin are critical in dermatology, cancer research and plastic surgery.

Pulse oximetry, based on near-infrared spectroscopy (NIRS), is currently the most widely used clinical technique for the measurement of blood oxygenation *in vivo*. This technique lacks spatial resolution (Kamat 2002), and yields only single point measurements of arterial blood oxygenation. Several other imaging modalities, such as magnetic resonance imaging (MRI), electron paramagnetic resonance imaging (EPRI), positron emission tomography (PET) and single photon emission computed tomography (SPECT), can also quantify blood oxygenation levels. Nonetheless, there are several disadvantages associated with each of the aforementioned techniques, the most common being their requirement of contrast agents to yield functional information.

Photoacoustic (PA) imaging involves the detection of acoustic waves that are generated by thermal expansion following optical energy absorption by a sample. The pressure generated is directly proportional to the local optical energy density absorbed in the tissue; hence, multi-wavelength PA measurements can yield optical spectral information. Accordingly, PA imaging has the potential for localized measurements of blood oxygenation levels (sO_2) (Wang *et al* 2003, 2006, Zhang *et al* 2006, Stantz *et al* 2006), expressed as a ratio of oxygenated haemoglobin concentration, $[HbO_2]$, to total haemoglobin concentration ($[HbO_2]+[HbR]$).

One way of quantifying blood oxygenation level from photoacoustic measurements *in vitro* utilizes the associated exponential rise in PA signals (Esenaliev *et al* 2002). The advantage of this approach is that it is self-calibrating as it deals with the relative change in the amplitude of PA signals rather than their absolute values. Performed at several optical wavelengths, this method can yield accurate values of sO_2 , independent of the surrounding tissue properties. However, this method requires that the absorbing volume be of a simple and predictable shape, for example, halfspace with planar boundaries, which is not feasible for *in vivo* micro-vascular imaging. Moreover, *in vivo*, the PA signals generated by the nearby blood vessels can have peaks occurring during the time decay of the PA signal of interest, thus dramatically affecting the sO_2 inversion.

Correspondingly, to perform *in vivo* functional imaging at the micro-vascular level, one has to develop a method for extracting quantitative spectral information from other features of the PA signals. The peak amplitudes of PA signals, which can unambiguously be attributed to different internal structures and are separable in the time domain, can be utilized for this purpose (Laufer *et al* 2006).

The peak amplitudes of the PA signals depend on the incident fluence, which can be controlled at the tissue surface, but has a depth-dependent distribution inside the tissue due to absorption of light by the capillary network and tissue light scattering. Hence, the knowledge of the optical properties of the tissue is vital for functional measurements using the PA imaging modality. While tissue optical properties can be measured *in situ* by optical measurement methods such as oblique-incidence optical fibre reflectometry (Lin *et al* 1997), such combined measurements can be effective only if the PA signal amplitude depends on the optical absorption coefficient of blood in a linear fashion. At the same time, the shape and amplitude of the PA signal depends on the optical energy deposition distribution in the blood vessel, which in turn is a function of light absorption, scattering and vessel geometry. Such dependences impose certain conditions only under which the PA signal amplitude is linearly proportional to the optical absorption coefficient of blood.

Hence, the first step is to investigate the relationship between the PA signal amplitude and optical absorption coefficient of the absorbing sample. Furthermore, the determination of blood oxygenation level from the measured PA spectrum is an inverse problem. The inverse problem must be solved without multiplying the measurement errors further and this places

additional limitations on the choice of optical wavelengths that can be used for imaging and needs to be studied.

Finding optimal experimental parameters for PA sO₂ measurements is the subject of this paper.

2. Theory and analysis

Several parameters can influence the shape and amplitude of photoacoustic signals. These include sound absorption in biological media, vessel (assumed to be of cylindrical shape) diameter, ultrasonic transducer focal position, and the illumination condition, which itself is a function of depth, tissue optical absorption coefficient, μ_a , reduced scattering coefficient, μ'_s , and tissue structure and inhomogeneity.

It is reasonable to assume that experimentally measured PA signal, A_k , which can be, for example, positive peak or peak-to-peak voltage or peak amplitude of the Hilbert transform of transducer voltage, is a unique function of some tissue parameters, p_α , including HbR and HbO₂ concentrations, and optical wavelength, λ_k . Let us suppose that the PA signal can be theoretically calculated from known p_α . Then, to find the tissue parameters, we need to solve the inverse (parameter estimate) problem.

Inverse problems are prone to be unstable, causing small errors in measurements to give large variances in inverted parameters. So, let us first consider the precision of the inverse solution based on the known optical spectra of HbR and HbO₂, to confirm the possibility of calculating sO₂ from wavelength-dependent PA measurements.

Parameter estimate problems are typically solved by minimizing the difference between the experimental PA signals, $A_k^{(e)}$, and the theoretical PA signals, $A_k(p_\alpha)$, in the least-squares sense, that is, ‘true’ parameters are those which minimize the relative error, E^2 :

$$E^2 = \frac{(A_k^{(e)} - A_k(p_\alpha))(A_k^{(e)} - A_k(p_\alpha))}{A_i^{(e)} A_i^{(e)}}. \tag{1}$$

An implicit sum over repeated small indices is assumed throughout this paper, and the least-squares difference has been normalized by the signal power, $A_i^{(e)} A_i^{(e)}$. If a minimum of E^2 is found by some minimization procedure, the linear term of the Taylor series expansion can be used near the minimum of E to estimate the error in the inverted parameters:

$$E^2 = \left(\frac{\delta A_k^{(e)}}{\sqrt{A_i A_i}} - S_{k\alpha} \left(\frac{\delta p}{p} \right)_\alpha \right) \left(\frac{\delta A_l^{(e)}}{\sqrt{A_j A_j}} - S_{l\beta} \left(\frac{\delta p}{p} \right)_\beta \right), \quad S_{kA} = \frac{\partial A_k}{\partial p_A} \frac{p_A}{\sqrt{A_i A_i}}, \tag{2}$$

where S_{kA} are sensitivities of the PA signal at wavelength k to parameter A

Taking into account that at the minimum, the partial derivatives of E with respect to any parameter are equal to zero, one can relate the relative error in the measured PA signal $\delta A_k^{(e)} / \sqrt{A_j A_j}$ to the relative change in the tissue parameters $(\delta p / p)_\beta$:

$$S_{\alpha k} \frac{\delta A_k^{(e)}}{\sqrt{A_j A_j}} = S_{\alpha k} S_{l\beta} \left(\frac{\delta p}{p} \right)_\beta. \tag{3}$$

Equation (2) represents a linear regression problem for parameter variance. Following Yapura *et al* (2004) in the assumption of wavelength-independent additive measurement errors, the statistical bounds for inverted tissue parameters can be obtained from the residual value of E at convergence:

$$\frac{\delta A_k^{(e)} \delta A_k^{(e)}}{A_i A_i} = \left(\frac{\delta p}{p} \right)_\alpha (S_{\alpha k} S_{k\beta}) \left(\frac{\delta p}{p} \right)_\beta = \frac{\eta}{n - \eta} \bar{E} F_{\eta, n-\eta}^{(1-\gamma)}, \tag{4}$$

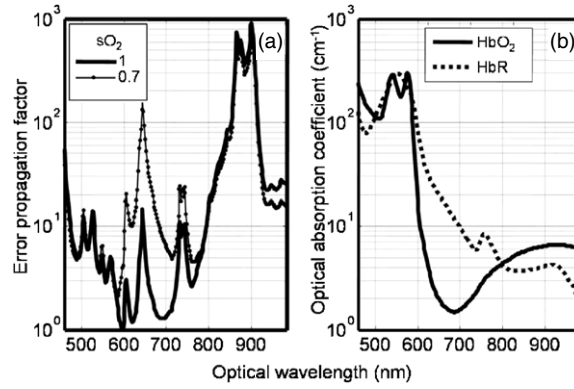


Figure 1. (a) Error propagation factor (EPF) for the inversion of sO_2 at different optical spectral bands. EPF is shown for sO_2 values of 100% (1) and 70% (0.7); (b) optical absorption spectra of HbR and HbO₂ for haemoglobin concentration typical in whole blood.

where $F_{\eta, n-\eta}^{(1-\gamma)}$ is an F -ratio distribution with η , $n - \eta$ degrees of freedom for a given confidence level, γ ; (Lewicki and Hill 2006), n is the number of wavelengths used and η is the number of independent parameters. Consequently, the variance bounds δp_B of a single parameter, say p_B , can be found from

$$\delta p_B^2 = \bar{E} \frac{\eta}{(n - \eta)} \frac{F_{\eta, n-\eta}(1 - \gamma)}{(C_{BB} - C_{B\xi} C_{\xi\xi}^{-1} C_{\xi B})}, \quad (5)$$

where $C_{\beta\alpha} = S_{\beta k} S_{k\alpha}$, $B = 1, 2, \dots, \eta$ and $\xi, \zeta = 1, 2, \dots, B - 1, B + 1, B + 2, \dots, \eta$. The error in the inverted parameter given by equation (5) increases with an increase in the number of unknown parameters, decreases with the number of measurements at different optical wavelengths, and depends on the combination of sensitivities S_{jk} , defined by the theoretical model used to calculate the PA signal.

The PA signal from blood samples *in vitro* can be calculated from the molar extinction coefficients, $\varepsilon_{a, \text{HbR}}(\lambda)$ and $\varepsilon_{a, \text{HbO}_2}(\lambda)$, and the concentrations of HbR and HbO₂, respectively, using a linear model (Laufer *et al* 2005):

$$\begin{bmatrix} A_{\lambda_1} \\ A_{\lambda_2} \\ \vdots \\ A_{\lambda_n} \end{bmatrix} = K \begin{bmatrix} \varepsilon_{a, \text{HbO}_2}(\lambda_1) & \varepsilon_{a, \text{HbR}}(\lambda_1) \\ \varepsilon_{a, \text{HbO}_2}(\lambda_2) & \varepsilon_{a, \text{HbR}}(\lambda_2) \\ \vdots & \vdots \\ \varepsilon_{a, \text{HbO}_2}(\lambda_n) & \varepsilon_{a, \text{HbR}}(\lambda_n) \end{bmatrix} \cdot \begin{bmatrix} [\text{HbO}_2] \\ [\text{HbR}] \end{bmatrix} = \mathbf{M}_{j\alpha} p_\alpha, \quad sO_2 = \frac{p_1}{p_1 + p_2} \quad (6)$$

where K is an unknown coefficient of proportionality between the heat deposition and the PA signal magnitude, which is assumed to be wavelength independent. Equation (6) constitutes a linear regression problem with the well-known solution:

$$p_\alpha = (\mathbf{M}_{\alpha i}^T \mathbf{M}_{i\beta})^{-1} \mathbf{M}_{\beta k}^T \Delta A_k. \quad (7)$$

The error propagation factor (EPF) for sO_2 is estimated by plugging in the solution of equation (6) into equations (2) and (5).

Figure 1(a) shows the EPF for the sO_2 inversion plotted as a function of wavelength for sO_2 levels of 100% and 70%. A moving set of four wavelengths, spaced 6 nm apart, was used for the inversion (x coordinate in figure 1(a) is the shortest of the set of wavelengths used for computation). The optical absorption spectra of HbR and HbO₂ for the typical haemoglobin

concentration found in whole blood are shown in figure 1(b) for reference. EPF has several distinct minima, notably around 580 nm, 785 nm and 1000 nm. Minima near 600 nm and 700 nm quickly disappear with a decrease in sO_2 .

Haemoglobin absorption at wavelengths longer than 600 nm is almost two orders smaller in magnitude than at 575 nm. Consequently, at longer wavelengths, (a) the signal-to-noise ratio degrades and (b) the influence of other absorbers, including water, becomes much stronger. Moreover, at longer wavelengths, the light scattering in blood can exceed the optical absorption and, hence, complicate sO_2 inversion from PA measurements. Although the EPF shows multiple minima, for the reasons stated above, the spectral range of 578–596 nm is chosen for *in vivo* sO_2 measurements. This choice of a narrow spectral region not only decreases measurement time but also minimizes the influence of other possible absorbers, such as melanin, which have weak, yet noticeable, spectral dependence.

For *in vitro* measurements, signal averaging significantly improves the signal-to-noise ratio and, consequently, the errors in measurements are systematic ‘modelling’ errors that emerge from sources such as unaccountable spatial light variations, imperfectness of the theoretical model, and/or the influence of other blood constituents. Unlike additive errors that are caused by random noise, systematic errors are multiplicative i.e. they are proportional to the photoacoustic signal magnitude. In this case, minimization of the weighted error function (normalized by the photoacoustic signal magnitude at each wavelength) should produce a more accurate parameter inversion.

In equation (6), we assume that the PA signal is linearly proportional to the absorption coefficient (μ_a) of haemoglobin and optical fluence (Φ) at the blood vessel surface. Due to the nature of equation (6), it is not possible to obtain correct absolute values for [HbR] and [HbO₂], and hence, the calculation of sO_2 becomes impossible in the cases of nonlinear dependence. This assumption holds only in the case of small light absorption, that is when $\mu_a a \ll 1$, where a is the vessel radius. Under this condition, a change in the fluence within the blood vessel caused due to haemoglobin absorption can be ignored. However, since the signal-to-noise ratio is the limiting factor for *in vivo* measurements, such small blood vessels are not clearly detectable and hence quantitative spectral measurements are difficult. Consequently, the development of a technique for sO_2 inversion for highly absorptive objects, when much of the laser energy is absorbed by the blood, is desirable.

The instantaneous ultrasonic pressure P_0 is proportional to the heat deposition, $\mu_a \Phi$, thermal expansion coefficient, β , stiffness, c^2/ρ (where c is sound speed) and inversely proportional to heat capacity ρC_p , $P_0 \sim c^2 \cdot \beta \cdot \mu_a \Phi / (C_p)$. At maximum optical fluence within ANSI safety standards, $\Phi \leq 20 \text{ mJ cm}^{-2}$, the peak photoacoustic pressure in soft tissue must be less than $P_0 \sim 10^6 \text{ Pa}$ where $c \sim 1.5 \text{ km s}^{-1}$, $C_p \sim 4.2 \text{ kJ kg}^{-1}$, $\rho \sim 10^3 \text{ kg m}^{-3}$, $\mu_a < 300 \text{ cm}^{-1}$, (blood at 574 nm), $\beta \sim 0.0002$. The corresponding acoustic Mach number is $M = P_0/\rho c^2 \sim 10^{-3}$. Since biological tissue is ultrasonically non-dispersive, ultrasound generation and further propagation of the attenuating sound waves can be treated as linear. Hence, the PA signal can be calculated as the convolution of acoustic pressure with the transient response of the ultrasonic transducer. The transducer response is measured by recording the time-domain signal from an optically absorbing acoustically thin cylinder ($a \ll \Lambda$, where Λ is the ultrasonic wavelength corresponding to the transducer central frequency) placed in the transducer focal plane, normal to the transducer axis. The shape of the measured transducer response (figure 2(b)) resembles that of the well-known Mexican-hat wavelet, which is typical of heavily damped ultrasonic systems without multiple longitudinal reflections and frequency dependence of group velocity (Kaspersen *et al* 2005).

The theoretical calculation of photoacoustic pressure that is caused by the instantaneous heating of a confined volume of optical absorber at a distance far from it can be found in the

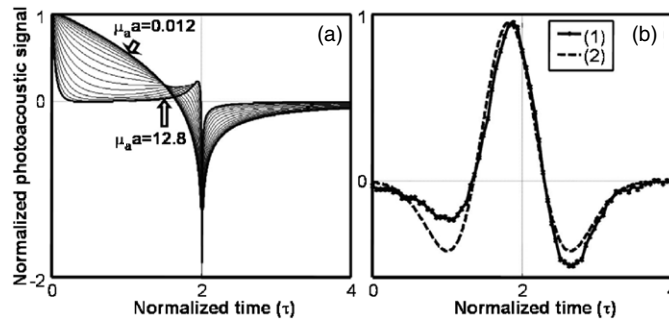


Figure 2. (a) Calculated photoacoustic pressure at a large distance from a uniformly illuminated cylinder for normalized absorption coefficients ($\mu_a a$) changing exponentially from 0.012 to 12.8 in incremental steps by a factor of $\sqrt{2}$, (b) experimentally measured transducer pulse response at $\Lambda = 2a$ (1) and Mexican-hat wavelet (2).

literature (Xu and Wang 2002, Diebold *et al* 1991). A closed form solution for the cylindrically symmetric case, which best represents blood vessels, is given as (Diebold *et al* 1991)

$$p(\xi, \tau) = \int_{-\infty}^{\tau-\xi} \frac{f'(\eta) + f'(-\eta)}{[(\tau-\eta)^2 - \xi^2]^{1/2}} d\eta \quad \text{with} \quad f(\eta) = \frac{-\beta c^2}{\pi C_p} \int_{\eta}^{\infty} \frac{\xi H(\xi)}{[\eta^2 - \xi^2]^{1/2}} d\xi. \quad (8)$$

Instantaneous heat deposition for a homogeneous cylinder uniformly illuminated by omnidirectional scattered light can be calculated directly as

$$H(\hat{\mu}_a, \xi) = \frac{\hat{\mu}_a I_o}{\pi} \int_0^{\pi/2} \int_0^{\pi} \exp(\hat{\mu}_a(\xi \cos \theta - \sqrt{1 - (\xi \sin \theta)^2}) / \sin \varphi) \cos \varphi d\theta d\varphi. \quad (9)$$

In equations (8) and (9), $\xi = r/a$ and $\tau = tc/a$ are the normalized distance from the centre of a cylinder of radius a , and the normalized time, respectively. Results of the calculations obtained from equations (8) and (9) are presented in figure 2(a). It can be seen that the time-domain pressure variation at a large distance from a uniformly illuminated cylinder, normalized by its own positive maximum, increases almost linearly with an increase in μ_a . In figure 2(a), the different curves represent different normalized absorption coefficients ($\mu_a a$) that change exponentially from 0.0175 to 12.8, incrementally by a factor of $\sqrt{2}$.

The results of convolution of the solution of equation (8), shown as solid lines in figure 2(a), with experimentally measured transducer transient response (figure 2(b)) are shown in figure 3. Figure 3 shows the peak PA signal amplitude plotted against the optical absorption coefficient normalized by the ultrasonic wavelength, Λ , for different normalized cylinder radii (solid lines change to dashed at $\mu_a a = 1$). As one can see, the PA signal amplitude depends linearly on the optical absorption coefficient when $\mu_a a \ll 1$. At high ultrasonic frequencies, such that $a \gg \Lambda$, the region of linear dependence of the PA signals can be extended up to $\mu_a \Lambda < 1$. The latter limit does not depend on the radius of the cylinder and hence, obviates the need for *a priori* knowledge of the vessel geometry. Moreover, this means that by choosing ultrasonic transducers of appropriate central frequencies and suitable optical wavelengths, one can get reasonable quantitative information even in the case of high optical absorption, $\mu_a a > 1$, albeit for the price of lower penetration depth of PAM.

It is also interesting to note that for $a \ll \Lambda$, the PA signal amplitude is proportional to the cross-sectional area of the cylinder. This enables PA microscopy to be used for relative measurements of blood volume in small vessels. For large diameter cylinders, the PA signal amplitude is proportional to the square root of the cylinder radius and hence,

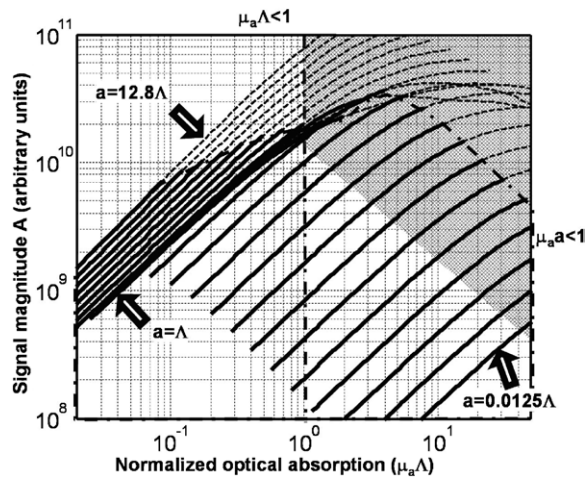


Figure 3. Peak magnitude of the photoacoustic pressure at a large distance from a uniformly illuminated cylinder as a function of optical absorption coefficient normalized by the acoustic wavelength ($\mu_a \Lambda$) for different normalized cylinder radii (solid lines change to dashed at $a > \Lambda$). Non-shaded portion indicates the region in which PA signal amplitude linearly depends on optical absorption coefficient. This holds when $\mu_a a \ll 1$ and at high ultrasonic frequencies, $a > \Lambda$, when $\mu_a \Lambda < 1$.

similar measurements to yield blood volume are prone to errors. However, at $a \gg \Lambda$, the photoacoustic (PA) signals from the two sides of the cylinder become separable in the time domain. Since time measurements are more precise than amplitude measurements, it is possible to estimate blood volume from the PA measurements for large diameter vessels.

3. Experiments, results and discussion

3.1. Experimental set-up

The theoretical model discussed previously for PA signal amplitude calculation is approximate; correspondingly, experimental verification is needed to justify the measurement precision. The PAM system used to acquire our data is shown in figure 4 and has been described previously in detail (Maslov *et al* 2005, Maslov and Wang 2005). A tunable dye laser (ND6000, Continuum) pumped by an Nd:YAG laser (Brilliant B, Bigsky), operating at 532 nm, providing 6.5 ns pulses at the rate of 10 Hz, was used as the light source. The irradiation pulses were coupled to a fibre optic cable. The incident light pulses were expanded by a conical lens and then focused onto the sample by an optical condenser with an NA of 1.1. The laser fluence incident on the sample surface was controlled to about 3 mJ cm^{-2} , which is well within the maximum permissible exposure of 20 mJ cm^{-2} set by ANSI standards (ANSI 2000). The signal detection and recording system consisted of a spherically focused ultrasound transducer (Panametrics) placed in a confocal arrangement with the optical illumination, a low noise amplifier and a digital oscilloscope (TDS 5034B, Tektronix). A computer-controlled three-dimensional mechanical scanner allowed precise positioning of the illumination and detection systems for raster scanning along the x - y plane with a set step size. Time histories of the PA signals were recorded at each position along the tissue surface to form so-called A-lines. The peaks of the A-lines are related to the boundaries of the optically absorbing structures, the peak amplitudes

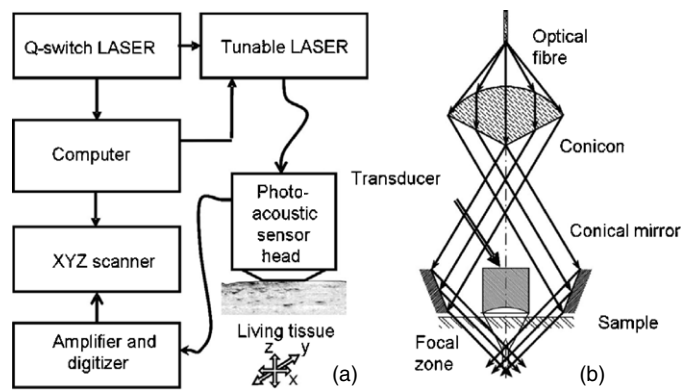


Figure 4. Schematic of the photoacoustic microscope.

to the absorption coefficients, and the arrival times to the distance to the absorber along the ultrasonic transducer axis. The collection of consecutive A-lines plotted against the transducer position along the scanning axis, x , parallel to the skin surface, forms B-scan images. The collection of B-scans at different y positions forms full 3D images of the tissue interior. To minimize positioning errors, all spectral data for a single B-scan were acquired before moving on to the next cross-section. Each A-line was normalized by the incident laser pulse energy to correct for the instability in laser output. The various peaks along the A-lines were identified and the corresponding positive peak amplitudes at several optical wavelengths were used for a pixel-by-pixel calculation of the sO_2 using equations (6) and (7). Published values of the molar extinction coefficients for HbO_2 and HbR were used for the matrix inversion procedure (Prahl 2004, Zijlstra *et al* 2000).

With a 50 MHz, 0.44 NA, 80% bandwidth transducer, the photoacoustic microscope (PAM) is capable of *in vivo* imaging of skin vasculature up to a depth of 3 mm with a lateral resolution of 40–120 μm , depending on imaging depth, and an axial resolution of 15 to 30 μm (Maslov *et al* 2005, Maslov and Wang 2005). With the other transducers used in this study (25 MHz and 10 MHz; 0.22 NA and 90% bandwidth for both), the resolution degrades with the transducer central frequency and numerical aperture, in accordance with the well-known Rayleigh criterion.

Phantoms comprising optically transparent cylindrical plastic tubes (TYGON S-54-HL, Norton Performance Plastics) of 0.25 mm inner diameter immersed in water were filled with black ink samples (Velvet Black, Private Reserve Ink) of different concentrations. Single point measurements of the PA signals generated by the samples were obtained at the isosbestic wavelength of 584 nm with a 50 MHz, 0.44 NA transducer.

In vitro experiments were performed on bovine blood samples of different oxygenation levels to confirm the linearity of PA signals with respect to absorption coefficient and to test the validity of the inversion procedure. Two stock samples of fully oxygenated and deoxygenated blood were made by saturating bovine blood (citrate dextrose solution used as anti-coagulant) with pure oxygen at 6 °C and deoxidizing it in a carbon dioxide atmosphere at 36 °C, respectively. Four more blood samples of different oxygenation levels were prepared by mixing the two stock samples in predetermined volumetric ratios (Scheid and Meyer 1978). As a control, optical sO_2 measurements were made on haemolysed blood samples (0.5% saponin, Sigma-Aldrich) using a spectrophotometer (GENESYS 20, Thermo Electron) in the wavelength range of 700–1000 nm with a step size of 4 nm (Tsao *et al* 1955). For PA

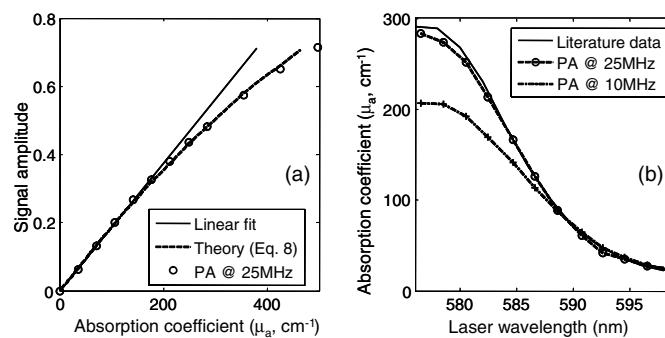


Figure 5. (a) Peak magnitude of the photoacoustic signal from a 0.25 mm diameter cylinder tube versus absorption coefficient for ink; (b) optical absorption coefficient versus laser wavelength for oxygen saturated whole bovine blood.

measurements, these blood samples were injected into optically transparent plastic TYGON tubes of 0.25 mm inner diameter, which were immersed in water. To avoid sedimentation, a steady flow of the blood samples was maintained through the tube at the rate of $\sim 0.1 \mu\text{l s}^{-1}$ using a syringe pump (Braintree Scientific). The other end of the tube was immersed in mineral oil to prevent any change in the $s\text{O}_2$ of the samples during the experiments. Two sets of single point PA measurements were acquired using the PAM system at 12 wavelengths between 576 and 598 nm in steps of 2 nm using the 25 MHz and 10 MHz transducers. The $s\text{O}_2$ level of each sample was calculated by using the PAM data and the published spectra of HbR and HbO₂, using a linear regression technique.

3.2. Results of phantom and *in vitro* blood experiments

Figure 5(a) shows a plot of the peak amplitudes of the experimentally measured PA signals from black ink samples of varying concentrations. Although the measurements were performed using a 50 MHz transducer, the central frequency from the measured signals was found to be near 25 MHz, due to frequency dependent ultrasonic absorption of 0.4 dB MHz^{-1} in tube material. The experimental data are in good agreement with the theoretical data. Moreover, both data coincide with a linear fit up to $\mu_a a \sim 2$.

Figure 5(b) compares the PA spectrum (from peak values of the PA signals) of the most oxygenated bovine blood sample obtained using 25 MHz and 10 MHz transducers with the reference spectrum (Zijlstra *et al* 2000). The experimental spectra were scaled by appropriate multiplicative factors to obtain the best fit. There is a good agreement between the PA spectrum measured with the 25 MHz transducer ($\mu_a \Lambda \sim 1$) and the reference HbO₂ absorption coefficient spectrum of bovine blood. For a longer ultrasonic wavelength, $\mu_a \Lambda > 1$, i.e. the PA signal obtained with a 10 MHz central frequency transducer does not show linear dependence on the optical absorption coefficient. The results of the *in vitro* experiments performed with bovine blood are consistent with the results obtained from phantom experiments and confirmed the linearity of the PA signals with respect to absorption coefficient for Λ such that $\mu_a \Lambda < 1$.

Energy deposition density is a linear function of light absorption in the case of weak absorption ($\mu_a a \ll 1$), but this is clearly not the best choice for photoacoustic measurements owing to a relatively low signal-to-noise ratio. Since peak light intensity on skin surface is limited by safety concerns, it is imperative to have effective sound wave generation by the object under consideration (blood), hence the $\mu_a a \sim 1$ requirement. However, by using an ultrasonic detector with central frequency high enough to satisfy the relation $\mu_a \Lambda \ll 1$, PA

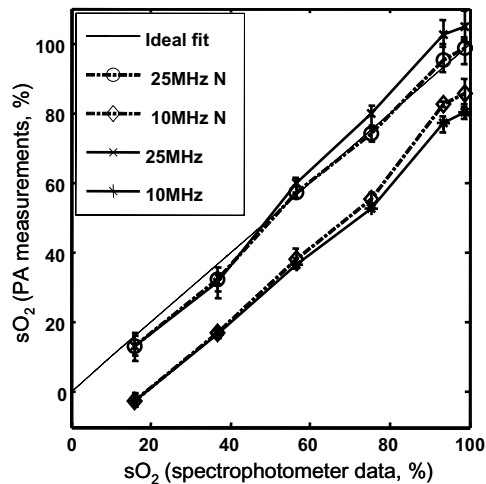


Figure 6. Comparison of inverted sO_2 values from *in vitro* photoacoustic measurements on whole bovine blood samples at different oxygenation levels using 25 and 10 MHz transducers versus those from optical measurements on corresponding chemically haemolysed samples. Dotted lines show sO_2 inversion results using normalized error function and solid lines show inversion results using non-normalized error function. Vertical bars represent data variance.

signal amplitude can be made to be a linear function of μ_a ; alternatively, for $\mu_a \Lambda \gg 1$, signal saturation occurs as has been shown experimentally.

Placing the tubes in turbid media (intralipid solution) did not change the experimental results significantly, except for the decrease in the PA signal amplitude due to additional attenuation of laser pulse (data not shown). This is not surprising because the size of the illumination spot was bigger than the diameter of the tubes used and the numerical aperture of the optical condenser exceeded the NA of the ultrasonic transducer by several times. Therefore, from a practical viewpoint, the optical illumination can be considered to be near omni-directional.

In figure 6, the PAM sO_2 measurements acquired using 25 MHz and 10 MHz central frequency transducers, are plotted against the NIR spectrophotometric sO_2 measurements on whole bovine blood samples of different oxygenation levels. The PA sO_2 measurements obtained with the 25 MHz transducer agreed with the spectrophotometric sO_2 data with a systematic error (accuracy) of 5%. The sO_2 data inverted from the PA measurements obtained with the 10 MHz transducer show a large (about 20%), although systematic shift to lower values. Variance in the PA measurements did not exceed 4%, and with signal averaging to reduce the influence of random noise, the variance decreased to about 1% (data not shown). This demonstrates the high sensitivity of PAM for measuring sO_2 . As has been noted before, with *in vitro* measurements, systematic error is the dominant source of errors, and a normalized error function is a better target function for minimization during sO_2 inversion. Figure 6 also compares the inversion results obtained using normalized (dash-dot lines) and non-normalized (solid lines) error functions. The results of such normalized inversions provide more accurate estimates of sO_2 with slightly smaller variances.

The effect of transducer focal position on the sO_2 measurements was found to be relatively small. With the 25 MHz transducer, the highest deviation in the sO_2 value measured at ± 0.5 mm from the transducer focus from that calculated at the focus, did not exceed 2%.

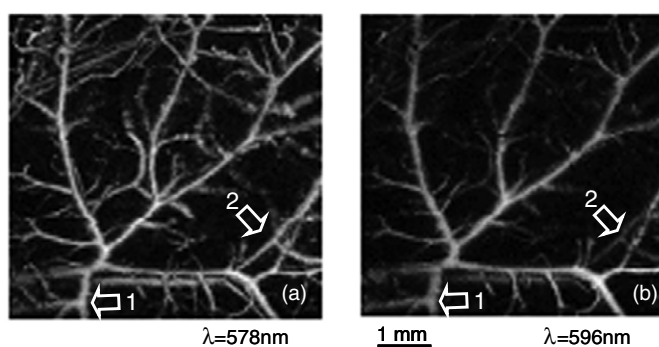


Figure 7. *In vivo* C-scan (maximum intensity projection) images of rat skin vasculature obtained using a 50 MHz ultrasonic transducer at (a) $\lambda = 578$ nm; (b) $\lambda = 596$ nm. sO_2 of vessel 1 (vein) is $50 \pm 10\%$ and vessel 2 (artery) is $75 \pm 10\%$.

3.3. *In vivo* measurements

In vitro studies demonstrated the linear dependence of the PA peak amplitude measurements on μ_a , and showed the high accuracy and sensitivity of PAM in the quantitative measurement of sO_2 within its realm of application ($\mu_a \Lambda < 1$). Based on this data, *in vivo* experiments were performed on Sprague Dawley rats (~ 200 g, Charles River Breeding Laboratories). All experimental animal procedures were carried out in conformity with the guidelines of the United States National Institutes of Health (NIH 1985). The laboratory animal protocol for this work was approved by the ULAC of Texas A&M University.

Before imaging, hair was removed from the back of the rat using commercial hair remover. Intramuscular injection of 87 mg kg^{-1} ketamine plus 13 mg kg^{-1} xylazine was administered to anaesthetize the rat, and the animal was kept motionless throughout the experiment with supplemental injections of a similar anaesthetic mixture ($\sim 50 \text{ mg kg}^{-1} \text{ h}^{-1}$). The area to be scanned was fixed using an in-house constructed holder and ultrasound coupling was provided using water and ultrasound gel. The body temperature of the animal was maintained at 38°C throughout the experiment. The arterial blood saturation and heart rate of the animal were monitored throughout the experiment using a pulse oximeter (Nonin Medical, Inc.). Spectral B-scan images were obtained at four wavelengths—578 nm, 584 nm, 590 nm and 596 nm. To obtain multi-wavelength PA data (using four wavelengths) over a $10 \text{ mm} \times 10 \text{ mm}$ area, it took about 200 min. The animal recovered without noticeable health problems after the experiment.

The C-scans (time gated maximum intensity projections, MIP) of the images acquired at the four different wavelengths were computed. These MIP matrices contained the peak amplitudes of the PA signals corresponding to absorbing structures on a pixel-by-pixel basis. These spectral peak PA values and the molar absorption coefficients of the oxy- and deoxy-haemoglobins of rat blood were used to invert for the sO_2 values.

Figures 7(a) and (b) show the C-scan (MIP) images of rat skin vasculature obtained using a 50 MHz ultrasonic transducer at $\lambda = 578$ nm and $\lambda = 596$ nm, respectively. It can be observed that some vessels, for example the one marked (1), have similar contrast at both 578 and 596 nm, while others (vessel 2), presumably an artery, practically disappear from the image taken at the longer optical wavelength. Vessels marked 1 and 2 on the image showed sO_2 of $50 \pm 10\%$ and $75 \pm 10\%$, respectively. Compared to these estimates obtained using a 50 MHz transducer, similar measurements taken with a 25 MHz transducer yielded estimates of sO_2 values that were $\sim 15\%$ to 20% lower. Further, measurements with a 10 MHz transducer

underestimated the sO_2 values by $\sim 25\%$ to 40% . Although the trends in sO_2 data inverted from PA measurements obtained with different central frequency transducers are consistent with theoretical predictions, they do not explain the significant underestimation of blood oxygenation level, which under normal conditions is expected to be about 98% for arterial blood and about 89% for venous blood (Kobayashi and Takizawa 1996). Blood oxygenation can drop with a decrease in vessel diameter (increase in branch order), which partly explains the underestimation of sO_2 in the microvasculature. However, there is also considerable sO_2 underestimation in relatively large diameter vessels (1). This indicates the presence of factors specific to *in vivo* measurements which influence the sO_2 results. Most plausibly, blood in the capillary network causes the optical fluence incident on the blood vessel to be spectrally dependent. Preliminary studies show that this effect can be accounted for and appropriate corrections can be made to *in vivo* sO_2 measurements (Maslov *et al* 2006), but only to certain extent. However, within the bounds of linear PA effect, simultaneous measurements of bulk tissue properties made by other, pure optical techniques can help improve the accuracy of sO_2 quantification from PA measurements *in vivo*.

4. Conclusion

We found that if the central frequency of an ultrasonic transducer is high enough such that the ultrasonic wavelengths are shorter than the light penetration depth into the blood in vessels, the PA signal amplitude is linearly proportional to the local optical absorption coefficient, making spectral measurements independent of the vessel size and position with respect to the ultrasonic transducer focus.

We showed that by choosing proper optical wavelengths, the error propagation factor defined as the ratio of errors in inverted parameters to the error in PA measurements (approximated by the standard deviation of measured PA signal values from values calculated at convergence) can be of the order of unity. We used the peak amplitude of spectral PA measurements in the wavelength range of $570\text{--}600\text{ nm}$, where error analysis showed minimal inversion error, to quantify blood oxygenation levels. High blood absorption in this wavelength region improves the signal-to-noise ratio and also minimizes the effect of optical scattering and absorption by other pigments. We have shown that in this wavelength range to obtain $\sim 4\%$ accuracy in *in vitro* sO_2 measurements, the central frequency of the ultrasonic transducer should be high enough to satisfy the relation $\mu_a \Lambda < 1$, that is, above 25 MHz for whole blood in this wavelength region.

In vivo oxygenation measurements of rat skin microvasculature show a similar dependence on ultrasonic frequency although the measured sO_2 was inconsistent with physiologically expected values. However, differences between the sO_2 values measured in arteries and veins were found to be within reasonable bounds, and the measured sO_2 value for arteries was within $\pm 25\%$ of the expected value of 98% . Consequently, by measuring the diffuse optical attenuation in tissue even with relatively low accuracy of about 20% , using techniques such as diffuse optical tomography, it would be possible to compensate for the spectral dependence of tissue optical attenuation, well enough to retain at least a few per cent accuracy in sO_2 measurements *in vivo*.

References

ANSI 2000 *American National Standard for Safe Use of Lasers* ANSI Standard Z136.1-2000 (New York: American National Standards Institute)

- Diebold G J, Sun T and Khan M I 1991 Photoacoustic monopole radiation in one, two, and three dimensions *Phys. Rev. Lett.* **69** 3384–7
- Esenaliev R A, Larina I V, Larin K V, Deyo D J, Motamedi M and Prough D S 2002 Optoacoustic technique for noninvasive monitoring of blood oxygenation: a feasibility study *Appl. Opt.* **41** 4722–31
- Gottrup F 2004 Oxygen in wound healing and infection *World J. Surg.* **28** 312–5
- Henke M, Bechtold C, Momm F, Dorr W and Guttenberger R 2000 Blood hemoglobin level may affect radiosensitivity—preliminary results on acutely reacting normal tissues *Int. J. Radiat. Oncol. Biol. Phys.* **48** 339–45
- Kamat V 2002 Pulse oximetry *Indian J. Anaesth.* **46** 261–8
- Kaspersen J H, Langø T and Lindseth F 2005 Wavelet-based edge detection in ultrasound images *Ultrasound Med. Biol.* **27** 89–99
- Kobayashi H and Takizawa N 1996 Oxygen saturation and pH changes in cremaster microvessels of the rat *Am. J. Physiol.* **270** H1453–61
- Laufer J, Elwell C, Delpy D and Beard P 2005 *In vitro* measurements of absolute blood oxygen saturation using pulsed near-infrared photoacoustic spectroscopy: accuracy and resolution *Phys. Med. Biol.* **50** 4409–28
- Laufer J, Elwell C, Delpy D and Beard P 2006 Absolute measurements of local chromophore concentrations using pulsed photoacoustic spectroscopy *Proc. SPIE* **6086** 60861J
- Lewicki P and Hill T 2006 *Statistics Methods and Applications* (Tulsa, OK: StatSoft)
- Lin S-P, Wang L, Jacques S L and Tittel F K 1997 Measurement of tissue optical properties by the use of oblique-incidence optical fiber reflectometry *Appl. Opt.* **36** 136–43
- Maslov K, Sivaramakrishnan M, Zhang H F, Stoica G and Wang L V 2006 Technical considerations in quantitative blood oxygenation measurement using photoacoustic microscopy *in vivo Proc. SPIE* **6086** 215–22
- Maslov K, Stoica G and Wang L V 2005 *In vivo* dark-field reflection-mode photoacoustic microscopy *Opt. Lett.* **30** 625–7
- Maslov K and Wang L V 2005 High-resolution photoacoustic vascular imaging *in vivo* using a large-aperture acoustic lens *Proc. SPIE* **5697** 7–14
- NIH 1985 *Guide for the Care and Use of Laboratory Animals* (Washington, DC: US Government Printing Office)
- Prahl S A 2004 *Optical Absorption of Hemoglobin* <http://omlc.ogi.edu/spectra/hemoglobin/index.html>
- Scheid P and Meyer M 1978 Mixing technique for study of oxygen-hemoglobin equilibrium: a critical evaluation *J. Appl. Physiol.* **45** 818–22
- Stantz K M, Liu B, Cao M, Reinecke D, Miller K and Kruger R 2006 Photoacoustic spectroscopic imaging of intra-tumor heterogeneity and molecular identification *Proc. SPIE* **6086** 608605
- Tsao M U, Sethna S S, Sloan C H and Wyngarden L J 1955 Spectrophotometric determination of the oxygen saturation of whole blood *J. Biol. Chem.* **217** 479–88
- Venkatesh B, Meacher R, Muller M J, Morgan T J and Fraser J 2001 Monitoring tissue oxygenation during resuscitation of major burns *J. Trauma* **50** 485–94
- Wang X, Pang Y, Ku G, Xie X, Stoica G and Wang L H 2003 Non-invasive laser-induced photoacoustic tomography for structural and functional imaging of the brain *in vivo Nat. Biotech.* **21** 803–6
- Wang X, Xie X, Ku G, Stoica G and Wang L H 2006 Non-invasive imaging of hemoglobin concentration and oxygenation in the rat brain using high-resolution photoacoustic tomography *J. Biomed. Opt.* **11** 024015
- Xu M and Wang L V 2002 Time-domain reconstruction for thermoacoustic tomography in a spherical geometry *IEEE Trans. Biomed. Eng.* **50** 1086–99
- Yapura C L, Kinra V K and Maslov K 2004 Measurement of six acoustical properties of a three-layered medium using resonant frequencies *J. Acoust. Soc. Am.* **115** 57–65
- Zhang H F, Maslov K, Stoica G and Wang L V 2006 Functional photoacoustic microscopy for high-resolution and noninvasive *in vivo* imaging *Nat. Biotech.* **24** 848–51
- Zijlstra W G, Buursma A and van Assendelft O W 2000 *Visible and Near Infrared Absorption Spectra of Human and Animal Hemoglobin, Determination and Application* (Leiden: VSP)